

Supporting information

NiCo₂S₄ cocatalyst supported Si nanowires heterostructure for improved solar-driven water reduction: experimental and theoretical insights

S. Gopalakrishnan^{a,b}, Mihir Ranjan Sahoo^c, Avijeet Ray^d, Nirpendra Singh^e,

S. Harish^{b,f}, E. Senthil Kumar^b, and M. Navaneethan^{a,b*}

^a Nanotechnology Research Centre (NRC), SRM Institute of Science and Technology,
Kattankulathur- 603 203, Chennai, Tamil Nadu, India.

^b Functional Materials and Energy Devices Laboratory, Department of Physics and
Nanotechnology, SRM Institute of Science and Technology, Kattankulathur-603 203, India.

^c Harish-Chandra Research Institute, Prayagraj, India-211 019.

^d Department of Physics, Indian Institute of Technology Roorkee, Roorkee-247 667, India.

^e Department of Physics and Center for Catalysis and Separation (CeCaS), Khalifa University
of Science and Technology, Abu Dhabi 127 788, United Arab Emirates (UAE).

^f Graduate School of Science and Technology, Shizuoka University, 3-5-1 Johoku, Naka-Ku,
Hamamatsu, Shizuoka 432-8011, Japan

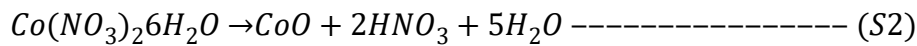
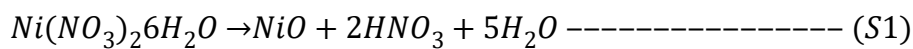
Corresponding authors

*Dr. M. Navaneethan

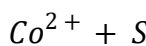
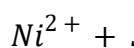
E-mail address: m.navaneethan@gmail.com

Formation of NiCo₂S₄ on Si NW surface

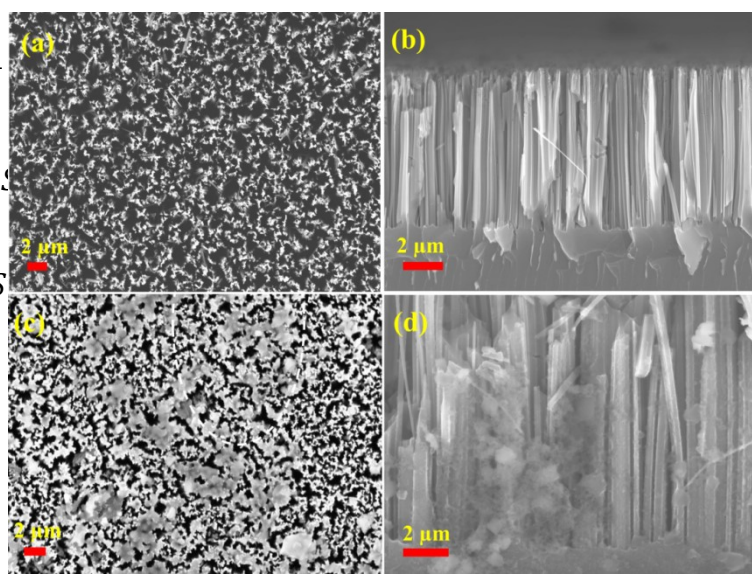
By dipping a substrate in aqueous solutions of Ni(NO₃)₂·6H₂O, Co(NO₃)₂·6H₂O, and Na₂S·9H₂O sequentially, NiCo₂S₄ thin films were created. SILAR is primarily based on ion by ion deposition, which manifests itself as deposition at nucleation sites on submerged Si NW surfaces. The following diagram depicts the growth mechanism of NiCo₂S₄ thin films grown using the SILAR method. When Ni(NO₃)₂·6H₂O, Co(NO₃)₂·6H₂O, and Na₂S·9H₂O are all dissolved in DDW water separately, the following three reactions occur.



In particular, the attraction between Ni²⁺ ions and the surface of Si substrate, when the Si substrate is immersed in the cationic precursor solution 1, Ni²⁺ ions begin to adsorb on the Si substrate. Here cohesive or van der Waals forces, as well as chemically attractive forces, might be existent to attach Ni²⁺ on the substrate. In a similar way, the Co²⁺ ions are adsorbed on Si substrate. Later, the immersion of Ni²⁺/Co²⁺ coated Si substrate into Na₂S anionic solution was the final phase of the reaction process. The Ni²⁺ and Co²⁺ ions react with S₂ ions from the Na₂S anionic solution during this reaction. The possible reactions are given as below equations.



Subsequently,



Na₂S

dissolves in water to yield S^{2-} ions, which are simultaneously hydrolyzed to produce HS^- and H_2S species. These molecules provide sulphur for the ion-exchange reaction that produces $NiCo_2S_4$ from Ni and Co precursors [1,2]

Fig. S1 FESEM micrographs of (a,b) top view and cross-sectional view of etched Si NW and (c,d) top view and cross-sectional view of Si NW/ $NiCo_2S_4$ NS.

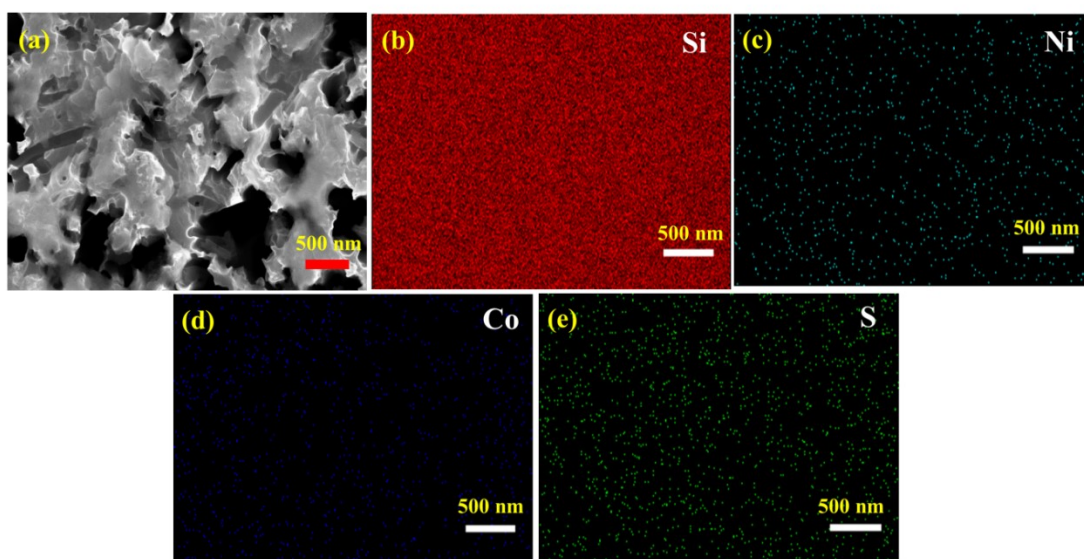


Fig. S2 (a) Top view of FESEM image of prepared heterostructure sample (b-e) EDS elemental mapping for Si,Ni,Co and S elements in Si NW/NiCo₂S₄ NS.

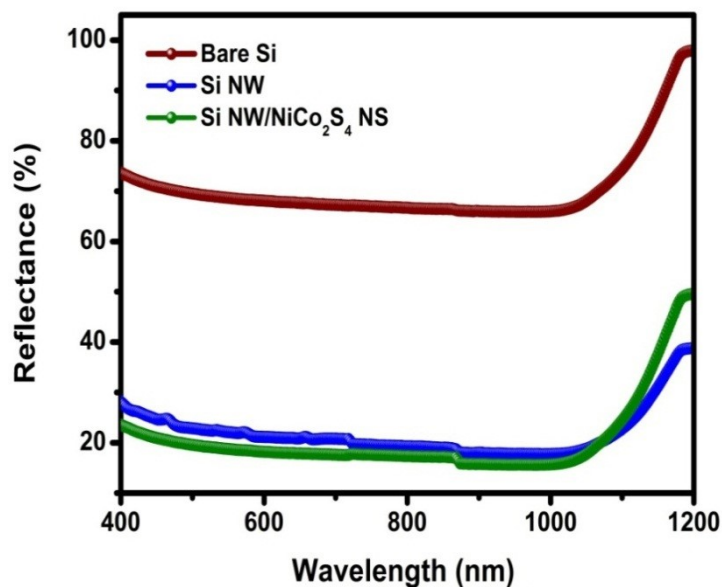


Fig. S3 UV-vis diffuse reflectance spectra of prepared samples

The anti-reflectance behaviour of prepared heterostructure against pristine Si NW has been performed using UV-Vis diffusion spectroscopy in the range of 300-800 nm. As shown in Fig.S4 the etched Si NW sample has a low reflectance property over the entire visible region owing to multiple internal reflectances within the vertical nanostructure geometry of the etched Si sample. On the other hand, the heterostructure and pristine samples determine the superior anti-reflectance properties over the visible region which is profitable to harvest more number of photons from solar spectrum. As a result, the NiCo₂S₄ NS contribution in anti-reflectance property is unchanged which is direct evidence to the material that retains its intrinsic anti-reflectance behaviour.

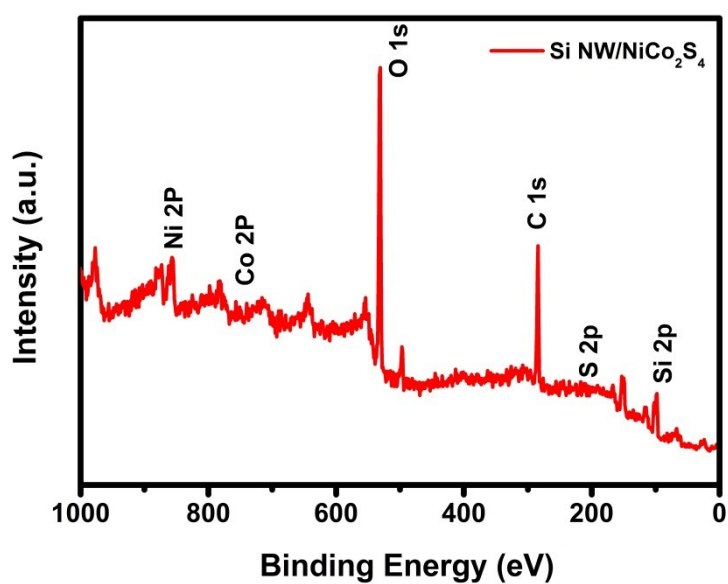


Fig. S4 XPS Survey spectrum of prepared heterostructure.

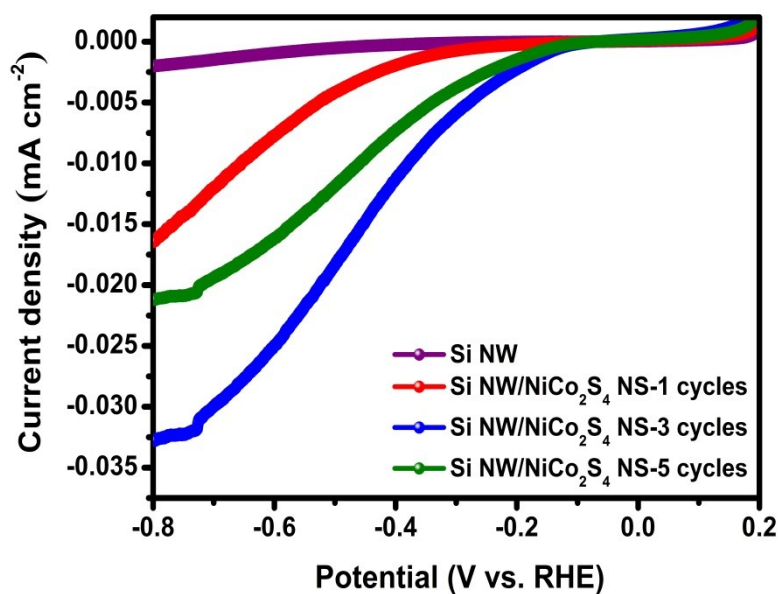


Fig. S5 Current density versus applied bias (vs. RHE) profile of prepared photocathodes under dark condition.

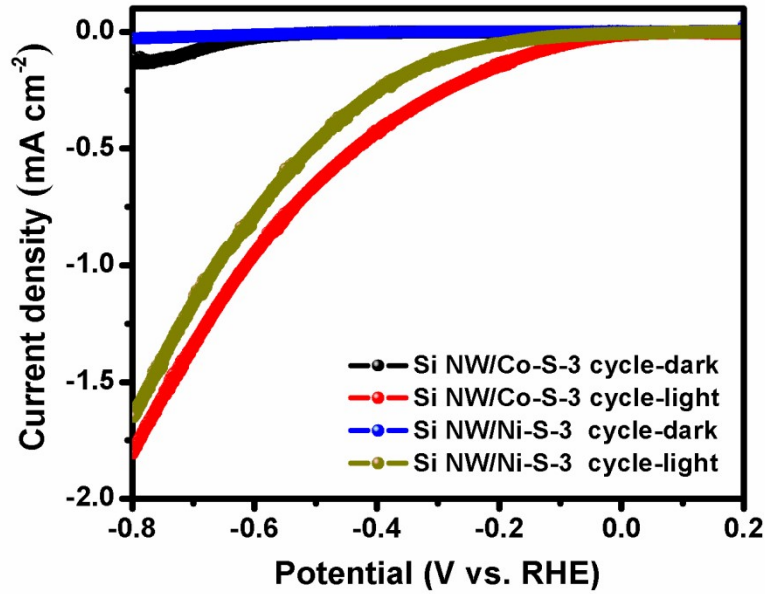


Fig. S6 Current density versus applied bias (vs. RHE) curves of prepared monometallic sulphide based photocathodes under dark and light conditions.

Faraday law of electrolysis equation

$$\text{Mole of } H_2 = \frac{1}{2F} \int_0^t I dt \text{ ----- (S7)}$$

where, F is the Faraday constant (Coulomb/one mole), I is the measurement of photocurrent density (mA cm^{-2}) and t is time (sec) [3].

The carrier lifetime of photoelectrode can be calculated from Bode plot using following equation (S8)

$$\tau = \frac{1}{2\pi f_{max}} \text{ ----- (S8)}$$

where, τ is lifetime of carrier, f_{max} = maximum peak frequency [4].

Photoelectrodes	Electrolyte	Current density J (mA cm ⁻²)	Applied bias (vs. RHE)	Reference
Si NW/NiCo ₂ S ₄ NS	1.0 M H ₂ SO ₄	15	-0.8 (vs. RHE)	Present work
pSi/Fe ₂ S ₂ (CO) ₆	1.0 M H ₂ SO ₄	2.8	-0.5 (vs. RHE)	5
5 mins etching of p-Si	HBr and liquid Br (4:1)	1.6	1.0 V (vs. RHE)	6
CuInS ₂ /Ag sensitized ZnO	Na ₂ SO ₃ +Na ₂ S	0.075	-	7
Si@CoSe ₂	1.0 M H ₂ SO ₄	11	-0.45 (vs. RHE)	8
C60/SnS ₂ -1.6/CuInS ₂	0.5 M of Na ₂ SO ₄	2.58	-0.45 (vs. RHE)	9
Cu ₂ Te/Cu	0.5 M Na ₂ SO ₄	-0.53	-0.5 (vs. RHE)	10
n-ZnO/P-Si NWs	Na ₂ SO ₄	-1.6	-1.5 (vs. RHE)	11
reduced graphene oxide/Si NWs	Na ₂ SO ₄	-4	1 (vs. Ag/AgCl)	12

Table 1: Comparison of PEC performances of fabricated heterostructure with previously reported photoelectrodes.

References

1. S.P. Ratnayake, J. Ren, E. Colusso, M. Guglielmi, A. Martucci and E. Della Gaspera, *Small*, 2021 **17** 2101666.
2. S.K. Shinde, S. Ramesh, C. Bathula, G.S. Ghodake, D.Y. Kim, A.D. Jagadale, A.A. Kadam, D.P. Waghmode, T.V.M Sreekanth, H.S. Kim and P.C. Nagajyothi, *Sci. Rep.* 2019, **9** 1-10.

3. N.H. Alvia, P.E.D.S Rodriguez, P. Aseev, V.J.G. Hernandez, A.H. Alvi, W. Hassan, M. Willander and R. Notzel, *Nano Energy*, 2015, **13**, 291.
4. F. Zhan, R. Xie, W. Li, J. Li, Y. Yang, Y. Li and Q. Chen, *RSC Adv.* 2015, **5**, 69753-69760.
5. S. Chandrasekaran, S., Vijayakumar, T. Nann, and N.H. Voelcker, *Int. J. of Hydrog. Energy*, 2016 **41** 19915-19920.
6. S.L. Wu, L. Wen, G.A. Cheng, R.T. Zheng and X.L. Wu, *ACS Appl. Mater. & Interfaces*, 2013 **5** 4769-4776.
7. Z. Cheng, X. Zhan, F. Wang, Q. Wang, K. Xu, Q. Liu, C. Jiang, Z. Wang and J. He, *RSC adv.* 2015 **5** 81723-81727.
8. C.J. Chen, K.C. Yang, M. Basu, T.H. Lu, Y.R. Lu, C.L. Dong, S.F. Hu and R.S. Liu, *ACS Appl. Mater. & Interfaces*, 2016 **8** 5400-5407.
9. F. Zhang, Y. Chen, W. Zhou, C. Ren, H. Gao and G. Tian, *ACS Appl. Mater. & Interfaces*, 2019 **11** 9093-9101.
10. D.J. Lee, G. Mohan Kumar, V. Ganesh, H.C. Jeon, D.Y. Kim, T.W. Kang and P. Ilanchezhian, *Nanomater.*, 2022 **12**, 3192.
11. A. Kargar, K. Sun, Y. Jing, C. Choi, H. Jeong, Y. Zhou, K. Madsen, P. Naughton, S. Jin, G.Y. Jung and D. Wang, *Nano let.*, 2013 **13** 3017-3022.
12. X. Zhong, G. Wang, B. Papandrea, M. Li, Y. Xu, Y. Chen, C.Y. Chen, H. Zhou, T. Xue, Y. Li and D. Li, *Nano Res.* 2015 **8** 2850-2858.